Giovanna Barigozzi[1], Claudio Mucignat[2], Hamed Abdeh[1], Davide Scandella[1], Giorgio Dolci[2]

Assessment of binary PSP technique for film cooling effectiveness measurement on nozzle vane cascade with cutback trailing edge

[1] Dipartimento di Ingegneria e Scienze Applicate - Università degli Studi di Bergamo

Viale Marconi 5, 24044 Dalmine (BG) Italy

[2] GE Power

Zentralstrasse 40, 5242 Birr, Switzerland

Corresponding author: Prof. Giovanna Barigozzi

Email: giovanna.barigozzi@unibg.it

Tel. +39 035 2052317

Mobile +39 347 5994525

Abstract

The present paper shows the results of an experimental investigation aiming to assess advantages and disadvantages of binary Pressure Sensitive Paints (PSP) technique for the measurement of film cooling effectiveness distribution. For this purpose, two test cases pertaining to gas turbine high pressure nozzle vane cooling systems have been used: a classical flat plate model with coolant injection through a single large scale shaped hole and a high loaded nozzle vane cascade with a pressure side cooling system that features two rows of cylindrical holes followed by a pressure side cutback with film cooling slots. Both models have been extensively tested: in particular, film cooling effectiveness data measured by means of well established thermal measurement techniques (Infrared thermocamera for the flat plate and wide banded Thermocromic Liquid Crystals for the vane cascade) are available from the literature. Pressure Sensitive Paints technique was able to provide high quality data all over the investigated test cases and operating conditions. Moreover, the binary version allows to fully eliminate any spurious temperature influence, thus making this technique well suited for the analysis of complex flows and geometries.

Keywords: PSP; gas turbine; film cooling; cutback trailing edge

1. INTRODUCTION

As well known, film cooling is a technique commonly used in gas turbines to protect the hot sections of the engine from the direct exposure to combustion products. Film cooling consists in ejecting a colder fluid, typically air coming from the compression section, through holes or slot in such a way to realize a layer that thermally protects the exposed surfaces from the hot gas. Film cooling is typically used both in the combustor to cool the liner and in the turbine, to cool both the airfoils and the platforms of high pressure stages . In the last decades an abundant literature has been produced on gas turbine film cooling, as its optimization is a key point to maximize gas turbine efficiency [1]. In fact, gas turbine efficiency maximization requires to minimize the cooling air consumption while improving the thermal protection of the exposed surfaces. The performances of a specific film cooling scheme are usually evaluated through the so called adiabatic film cooling effectiveness η and the convective heat transfer coefficient h, defined as follows:

$$\eta = \frac{T_{aw} - T_e}{T_c - T_e} \quad (1)$$

$$h = \frac{\dot{q}}{T_{aw} - T_w} \quad (2)$$

Where T_w is the wall temperature, T_{aw} is the wall temperature in case of an adiabatic process, T_c is the coolant temperature at the exit of the film cooling hole or slot, T_e is the main flow temperature and q is the local heat flux. The adiabatic film cooling effectiveness does not depend on coolant and main stream temperature values but depends on their mixing process, that in turns depends on the geometry of the cooling scheme and on coolant and main stream flow conditions. It is intended to provide information on the coolant distribution, and thus on its concentration, at the wall. Adiabatic film cooling effectiveness (and of course heat transfer coefficient) has been and still is typically measured using heat transfer based techniques, like Thermo-chromic Liquid Crystals (TLCs) or Infrared (IR) Thermography. Through this approach, a hotter or colder secondary stream is injected into the main flow, thus using temperature to trace the presence of coolant on the surface. The need to comply with adiabatic condition forces the researchers to use low conductive materials in the model manufacturing and/or to limit test duration, with the risk of not reaching a steady state solution. As a perfect adiabatic condition cannot be reached, especially when testing complex cooling geometries on engine scale components, conduction effects will be inevitable, especially close to injection location. Conduction effects can be of course mitigated up to a certain level but at the expense of highly complex procedures that typically involve a FEM computation to assess the heat conduction across the test model, which could be applied in testing simple geometries like flat plates or simplified models. However, if the test model has a 3D shape and the cooling scheme is complicated, such a correction procedure could become a difficult task.

Conduction effects on the other hand could be completely avoided when using measurement techniques that are based on the heat/mass transfer analogy, like the Ammonia-diazo technique [2] and, more recently, the Pressure Sensitive

Paints (PSP) technique [3]. As these paints are sensible to the oxygen partial pressure at the wall, they are readily at hand since inert gases as CO_2 or N_2 are commonly used in lab tests to model the correct density ratio of the film cooling jets with the main flow, usually air, so the traditional experimental facilities can be straightforwardly used. Hence, if coolant and main flow have the same temperature, heat transfer phenomena are totally avoided and a real adiabatic condition is established.

PSP are based on the absorption-emission principle due to oxygen quenching, and can be used with two kind of measurement principles: the lifetime method and the intensity based one [4]. The former requires to measure the decay time of luminescence (of the order of less than 20 μs) with gated intensified CCD cameras and it is suited to track fast phenomena. Intensity based methods are inherently simpler as they are based on the emitted light intensity. This technique is gaining a large popularity in the gas turbine heat transfer community, as in principle it allows to directly measure the adiabatic film cooling effectiveness, without the need of further conduction corrections and making use of scientific grade CCD cameras. A thorough discussion of the use of this kind of PSP technique in the film cooling research field can be found in the work of Han and Rallabandi [5]. In this review paper results from the application of single component PSP technique on a flat plate model as well as on airfoils and platforms, both in stationary and rotating condition, are put together to demonstrate the ability of this technique to provide detailed and accurate adiabatic film cooling effectiveness distributions on complicated geometries. In fact, Li et al. [6] have shown that, differently from TLC technique, PSP signal is practically unaffected by surface curvature, allowing to obtain useful data over complicated geometries. Moreover, opposite to IR Thermography, PSP technique does not require particular optical windows, making its application cheaper and easier.

Quantitative comparisons between PSP and heat transfer based techniques from flat plate testing are also available in the open literature. Wright et al. [7] compared PSP results against data from IR thermography considering a flat plate model cooled by a row of compound angle cylindrical holes injecting at 30° to the plate surface. The model was tested at low speed with variable coolant to mainstream blowing ratio and mainstream turbulence. Single luminophor steady state PSP technique was found to be superior, especially in the near hole exit region, where conduction effects typically affect IR based data. Similar conclusions were also drawn by Caciolli et al. [8] testing a multiperforated plate simulating a liner cooling system. In this case, steady state single component PSP technique was compared with wide banded TLC data, again demonstrating the capability of PSP to correctly capture the effects of the complex jet to mainstream interaction in the near hole exit region, unaffected by conduction. Other papers are devoted to the assessment of the uncertainty in PSP measurements. Liu et al. [9] performed a detailed theoretical investigation on the accuracy of pressure measurement, revealing that surface temperature has the largest impact on the uncertainty of the computed pressure value. Natsui et al. [10] performed a detailed analysis of the influence of experimental aspects like

test repeatability that might impact on the uncertainty of film cooling effectiveness values taken by using PSP technique, providing recommendations for testing methodologies able to minimize sources of potential errors. PSP technique has been also used in simplified models of trailing edge cooling slots [11-12], allowing to investigate the influence of slot internal geometry on the thermal protection of the cutback surface.

All these studies make use of single luminophor paints and refer to low speed testing conditions where temperature variations along the surface are not relevant. Only few applications of PSP technique in compressible flow condition are available. Zare-Behtash et al. [13] tested different formulations of single luminophor PSP technique to measure the pressure distribution along a 2D air ejector system. The same procedure for temperature correction proposed by [5] was adopted in this study. Liu et al. [14] performed film cooling effectiveness measurements on the rear suction side of a vane cascade in transonic condition looking for the influence of shock wave. Zhou et al. [15] tested a flat plate model cooled by a row of cylindrical holes at mainstream Mach number as high as 0.7. The reported calibration curves obtained for variable temperature collapsed when normalized using the reference pressure measured at each specific temperature. This means that a unique calibration curve can be used whenever the temperature gets constant between reference and testing conditions. The authors state that temperature variations as high as 5°C take place at high Mach number but the impact of this variation on measurement accuracy is not discussed. As temperature variations are expected to take place due to conduction and compressibility effects in complex geometries, the use of single-luminophor PSP can lead to uncertainty in the computed film cooling effectiveness values that can be avoided by the use of dual luminophor (binary) PSP [16]. Binary PSP contains a probe (pressure and temperature dependent) and a reference (temperature dependent) luminophor molecule. By computing the ratio of the light intensity emitted by these two molecules, an almost temperature independent pressure signal is obtained.

The present paper contributes to the existing body of literature in documenting the experimental activity carried out to develop binary PSP technique at the Energy System and Turbomachinery Laboratory of Bergamo University, Italy, in collaboration with General Electric Power Component & Development Test labs in Birr, Switzerland. The experimental activity initially consisted in the design, manufacturing and testing of calibration devices for single and dual-luminophor PSP. Once thoroughly calibrated, single and dual-luminophor PSP were critically assessed at GE Laboratory on a flat plate model cooled by means of shaped holes. Data available from IR thermography [17] at variable injection condition were used for validation. The same binary PSP technique was then used at Bergamo University on a linear vane cascade with a pressure side cooling system made of two rows of cylindrical holes followed by a cutback trailing edge. In this case literature data were used to prove the binary PSP technique on a complex geometry.

2. THE PSP TECHNIQUE

Pressure sensitive paints are made of luminescent molecules dispersed into a polymeric matrix. These paints absorb oxygen depending on pressure. Once excited with light with an appropriate wavelength (400 nm), the coating emits a radiation at a different wavelength (650 nm); the intensity of this radiation is inversely proportional to the amount of oxygen absorbed. This technique can be used to measure the pressure distribution or the oxygen concentration. The following concepts are taken from Jahanmiri [18]. Stern-Volmer equation gives the relationship between the luminescent intensity I and oxygen concentration c:

$$\frac{I_{max}(T)}{I(T)} = 1 + K(T) \cdot c \quad (3)$$

where I_{max} is the maximum intensity in absence of oxygen and K is the Stern-Volmer constant. It is worth noting that the intensity values and the Stern-Volmer constant are temperature dependent. Luminescent molecules are usually dispersed into a porous binder. According to the Henry's law, it is possible to relate the oxygen concentration within the binder to the pressure on the PSP surface:

$$c = S(T,p) \cdot X \cdot p \quad (4)$$

S being the Henry's law coefficient, a function both of temperature and pressure, X the mole fraction of oxygen in air and p the air pressure. From the above equations the following expression can be derived:

$$\frac{I_{ref}}{I} = A(T) + B(T) \cdot \frac{p}{p_{ref}} + C(T) \cdot \left(\frac{p}{p_{ref}}\right)^2 \quad (5)$$

where the *ref* subscript denotes a no flow condition, which means that pressure is constant over the whole surface. Polynomial constants A, B and C depend on temperature and must be defined through a calibration process.

To apply PSP technique to film cooling effectiveness measurement, the similarity between mass transfer and heat transfer is exploited. Instead of injecting a heated/cooled secondary stream, a foreign gas like nitrogen or carbon dioxide is injected at room temperature, thus in principle avoiding any heat conduction related problem. The intensity of light emitted by PSP will thus change depending on the amount of oxygen reacting with the luminescent molecules, that in turns depends on the mixing between air and foreign gas. By recording the light emitted by PSP during two tests, one injecting air ($(p_{O2})_{air}$) and one injecting nitrogen/CO_2 ($(p_{O2})_c$), and also acquiring the light emitted in the reference atmospheric condition (p_{ref}), the so called wind off image, adiabatic film cooling effectiveness can be computed as follows:

$$\eta = \frac{c_e - c_{mix}}{c_e} = 1 - \frac{1}{1 + \frac{MM_c}{MM_{air}}\left[\frac{\left(p_{O_2}/p_{ref}\right)_{air}}{\left(p_{O_2}/p_{ref}\right)_c} - 1\right]} \quad (6)$$

where c_e is the oxygen concentration into the mainstream and c_{mix} those in the mainstream-coolant mixture, MM_{air} and MM_c are the molecular weight of air and of coolant (N_2 or CO_2), respectively. Please note that a forth image is acquired

both during calibration and measurements, the so called dark image. This image is acquired with both the light and the flows off and it is used to correct for imperfections in the CCD camera sensor.

In conclusion, two are the major hypothesis over which PSP technique for film cooling effectiveness measurement is based on: i) the validity of heat/mass transfer analogy and ii) the minimization of temperature influence on pressure measurement.

2.1 Heat mass transfer analogy

The applicability of heat/mass transfer analogy has been deeply discussed by Han and Rallabandi [5]. Considering temperature and concentration boundary layer equations for steady, incompressible 2D flow with constant properties, some similarities between these equations can be identified, i.e. the presence of an advection term on the left-hand side and of a diffusion term on the right-hand side. For the heat/mass transfer analogy to be valid, the two dimensionless groups in the diffusion terms of temperature and concentration non dimensionalized boundary layer equations must be the same. This means that the Lewis number (*Le*), that is the ratio of Schmidt (*Sc*) and Prandtl (*Pr*) numbers, must equals 1:

$$Le = \frac{Sc}{Pr} = \frac{\alpha}{D_{AB}} = 1 \qquad (7)$$

where α is the thermal diffusivity and D_{AB} the molecular diffusion. The Lewis number is a measure of the relative thermal and concentration boundary layer thicknesses and it is relevant to any situation involving simultaneous heat and mass transfer by convection. It has to be observed that in principle the Lewis number to be equal to 1 asks for the presence of a fully turbulent boundary layer. Laminar or even transitional boundary layers do not guarantee the full applicability of heat/mass transfer analogy. In film cooling applications, the interaction between coolant and mainstream typically results in a turbulent flow condition right from injection location. Some exceptions could be for example the cooling of the leading edge (showerhead), where coolant is injected against the mainstream, and coolant injection through slot with smooth walls. In these cases a fully turbulent flow condition could not be reached over the whole investigated domain.

Heat/mass transfer analogy, relaying on the Lewis number, could be in principle affected by compressibility effects. The influence of compressibility on the validity of heat/mass transfer analogy has been addressed by Zhou et al. [15]. They have shown that this analogy is valid even at high Mach number as compressibility influences in a similar way the thermal diffusivity and the molecular diffusion, thus cancelling its influence on the Lewis number.

2.2 Temperature Influence

The second potential source of error derives from the assumption that mainstream, injected air and injected foreign gas should all have the same temperature, equal to the ambient temperature, i.e. the temperature taking place when the reference wind off image is acquired. In fact, the calibration curve that can be derived by inverting equation (5) and correcting for any camera defects through the Dark image, is temperature dependent:

$$\frac{p}{p_{ref}} = A(T)\left(\frac{I_{ref}-I_{Dark}}{I-I_{Dark}}\right)^2 + B(T)\left(\frac{I_{ref}-I_{Dark}}{I-I_{Dark}}\right) + C(T) \quad (8)$$

Typically each calibration is performed keeping a constant temperature while varying pressure. It is eventually repeated at a different temperature level, which stays constant during calibration. The resulting calibration curves do not coincide if a unique value of the reference pressure is used, and these differences increase with rising pressure, as will be shown in the calibration section. They instead coincide if a reference wind off image is recorded for each temperature tested. This means that, during measurement, uncertainty in the local adiabatic film cooling effectiveness can derive from at least two events: first, main flow and coolant flow do not have the same temperature and, second, if the reference condition has been acquired at a different temperature. The first effect is inversely proportional to the oxygen concentration, becoming higher where low film cooling effectiveness values are detected. The second effect could potentially affect the entire effectiveness distribution because it is an error on the reference. It becomes relevant for compressible flows, where significant temperature variations take place along the test model. To minimize this aspect, Han and Rallabandi [5] suggest to record the reference wind off image immediately after the end of each test, hoping that the surface temperature variation induced by flow temperature variation does not change significantly once the flow is switched off. As this will not be always the case, an alternative solution that allows to eliminate the influence of temperature must be included in the experimental methodology.

2.3 The binary PSP

Since the main source of error for single-luminophor pressure-sensitive paint is the temperature dependence, multi-luminophor PSP systems have been also developed with the purpose of compensating the temperature effect. Binary pressure sensitive paints are made of two kind of luminescent molecules dispersed into a binder. Similarly to single luminescent PSP, one of these paints (probe) absorbs oxygen depending on pressure and temperature while the other only depending on temperature (reference). Once excited with light with an appropriate wavelength (400 nm), the coating emits two different radiations: the first one at 650 nm (red - pressure and temperature dependent) and the second one, called reference signal, at 550 nm (green - temperature dependent). As no overlap exists between the emission spectra of the probe and reference luminophors, the luminescent emissions can be easily separated using band-pass optical filters. As the temperature dependency of the two luminescent paints almost coincides, the reference signal can

be used to compensate the temperature dependency of the probe signal. McLean [19] pointed out that since two luminophores cannot be perfectly mixed, the simple two-color intensity ratio $I_{\lambda 1}/I_{\lambda 2}$ cannot completely compensate the effect of non-homogeneous dye concentration. In this case, a ratio of ratios should be used to correct the effect of non-homogeneous dye concentration and paint thickness variation, as suggested by Liu and Sullivan [20]:

$$\frac{r_{ref}}{r} = \left(\frac{I_{ref}-I_{Dark}}{I-I_{Dark}}\right)_{650} \Big/ \left(\frac{I_{ref}-I_{Dark}}{I-I_{Dark}}\right)_{550} \quad (9)$$

The ratio r_{ref}/r is going to replace the intensity ratio I_{ref}/I in Equation (10).

Consequently, the setup is more complex as two filters and a filter holder, or better two CCD cameras, are required. Moreover, the test sequence has to be repeated twice or in parallel to get information from both the red and the green filters.

Different kind of PSP are available on the market. In the present investigation two kind of PSP were tested, both from ISSI:

- Uni FIB, a bright single-luminophor pressure sensitive paint (PSP) optimized for maximum luminescent signal while maintaining high pressure sensitivity and low, but not null, temperature sensitivity, and
- Binary FIB, a combination of a temperature-sensitive luminophor, which cannot be quenched by oxygen, and of an oxygen-sensitive luminophor, like the one of single-component PSP. Binary PSP can be considered almost temperature insensitive in a range of 5°C ÷ 45°C [20].

2.4 PSP calibration

Both single and dual component PSPs need to be calibrated to identify the relationship between light intensity and pressure (equation (8)). The calibration consists in recording a series of images of a target surface sprayed by PSP under controlled pressure and temperature conditions. A calibration device has been specifically designed and manufactured both in Bergamo and Birr Laboratories (Fig. 1). In Bergamo Laboratory (Fig. 1a), the target surface is installed above a Peltier cell to control its temperature and both are installed inside a sealed box. In Birr Laboratory (Fig. 1b) the target temperature is controlled by means of a heater and a cooling water circuit. In both cases pressure inside the sealed box can be varied from 0 bar up to 1.5 bar by a vacuum pump or compressed air. The target surface is illuminated by a 400 nm UV lamp while light intensity is acquired by CCD cameras through two band-pass filters. Two different setups are used: in Birr two CCD cameras are available (Lavision Imager Pro with a 1600x1200 resolution and a 14bit sensitivity), each one equipped with a band-pass filter, so the two signals will be acquired simultaneously (Fig. 1b) and then de-warped on a common spatial grid using algorithms mutated from the Particle Image Velocimetry technique. This is of course the best solution in terms of accuracy, as it allows the simultaneous acquisition of the two signals and the

optimal setting up of each camera. In Bergamo a unique CCD camera is available (FlowSense EO 4M with a 2048 x 2048 resolution and a 12bit sensitivity): a multiple filter holder has been designed and manufactured in order to fast changing the filter without moving the CCD camera (Fig 2). This of course does not allow the simultaneous acquisition of the two signals, red and green, but in steady state condition it can be acceptable. Concerning the setting of the camera, a compromise will be found between the red and the green signals, eventually sacrificing the green signal resolution. This in order to preserve the maximum resolution on the red signal, the one carrying the pressure information, in the meanwhile avoiding saturation.

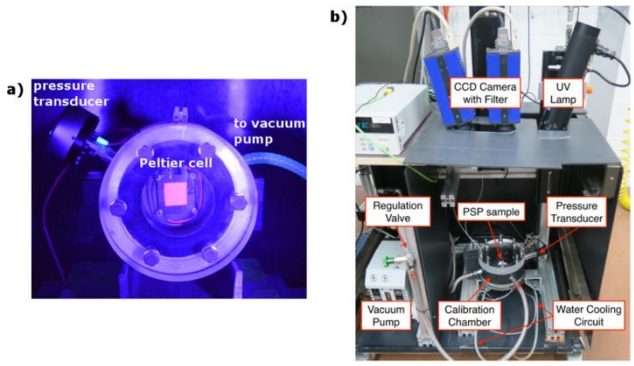

Fig 1 Calibration setup: a) at Bergamo Lab and b) at Birr Lab

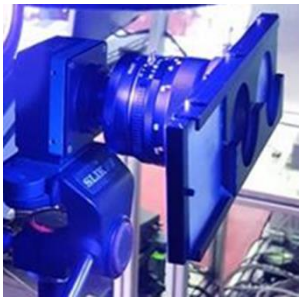

Fig 2 The filter holder

As previously mentioned, during the calibration process, temperature is kept constant while varying pressure: a set of 100 images is recorded at each pressure step and then averaged in order to minimize the influence of noise. In the meanwhile pressure and temperature are measured by an absolute pressure transducer (SETRA 204A 0-25 psia) and an RTD Pt100. The same procedure is repeated for different temperature levels. A further image is acquired in atmospheric condition and with the light switched off (I_{Dark}) to correct for any CCD camera defects. Figure 3 shows the calibration curves obtained for single and dual luminophor PSP for different target temperature from 15°C up to 35°C at Birr Laboratory. Please note that each curve in Fig. 3 has been obtained using the reference intensity measured at 20°C. As expected, temperature variation has an impact on single component PSP, with curves that tend to coincide approaching

the void. Conversely, dual component (binary) PSP show a behavior almost independent from temperature. When considering the application of PSP technique to the measurement of adiabatic film cooling effectiveness, one can conclude that temperature effects will be larger far from injection location, i.e. where high oxygen concentration will be measured. High η values will instead correspond to low oxygen concentrations, i.e. very low pressure ratios.

Figure 4 finally compares binary PSP calibration curves measured at Birr and Bergamo Laboratory with those declared by the manufacturer [21]. The different sets of data do not coincide, especially approaching the void, i.e. when light intensity is higher. This was related to the influence of the CCD camera performance, as different cameras were used in Birr and Bergamo experiments with a different resolution: 14bit (GE) and 12bit (Bergamo).

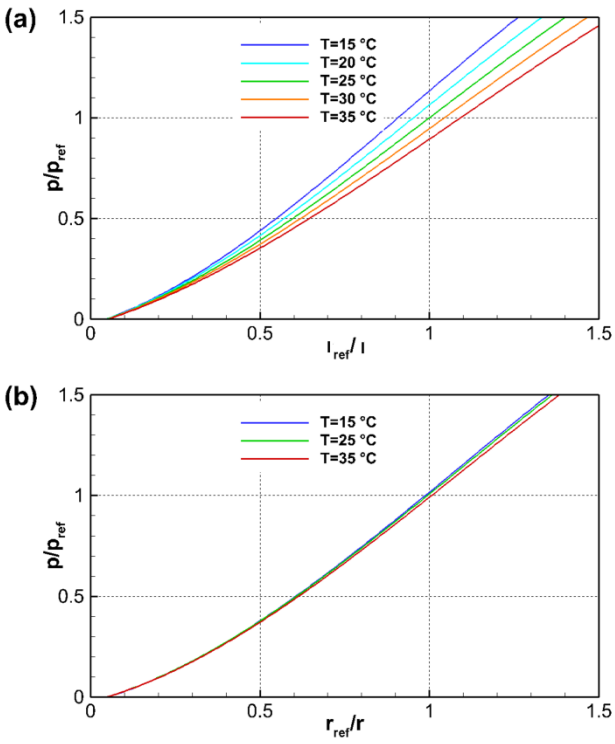

Fig 3 Calibration curves: a) single component and b) binary PSP

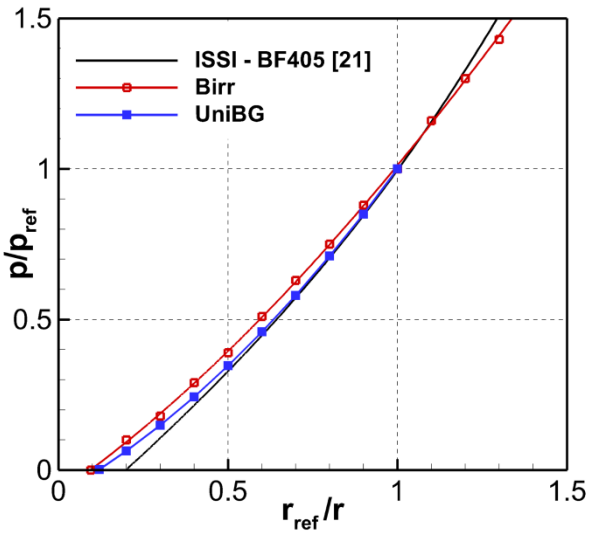

Fig 4 Comparison between binary PSP calibration curves from Birr and Bergamo Laboratories

2.5 Measurement uncertainty

The PSP technique provides the value of p/p_{ref} during the two tests over the investigated surface. The film cooling effectiveness measurement uncertainty depends on PSP calibration and image acquisition. In fact, from equation (6) the following expression for the uncertainty can be derived:

$$\delta\eta = \sqrt{\left(\frac{\partial\eta}{\partial(p/p_{ref})_c}\delta(p/p_{ref})_c\right)^2 + \left(\frac{\partial\eta}{\partial(p/p_{ref})_{air}}\delta(p/p_{ref})_{air}\right)^2} \quad (10)$$

But what is measured is the intensity level recorded by the CCD camera. The relationship between the recorded light intensity and the pressure ratio is obtained from calibration through equation (1). It is then possible to derive a similar expression for the uncertainty on the pressure ratio, that will depend on the uncertainty in the calibration constants *A*, *B* and *C* and in the CCD camera resolution. Finally, a quite complicated expression can be derived, showing that the uncertainty in the effectiveness value can be computed knowing the uncertainty of the pressure transducer used for calibration (δp = ± 189.6 Pa) and properly setting the CCD camera for maximum signal to noise ratio.

This computation results in a final uncertainty of $\delta\eta$ = ± 1.4 % with η = 0.5 and $\delta\eta$ = ± 15.6 % when η = 0.1.

3. THE FLAT PLATE TEST CASE

A first assessment of the PSP technique was conducted on a flat plate test case, comparing the PSP measured effectiveness with the one obtained with the well-known IR method. Both Uni FIB and Binary FIB coatings have been used to demonstrate the technique robustness in a test case where the heat and mass transfer analogy is well applicable.

3.1 Experimental details

Tests were performed in the wind tunnel for flat plate testing at the GE Laboratory in Birr, CH. This is a continuously operating wind tunnel delivering a main flow air up to 1 kg/s into a test section of 50 mm x130 mm cross section. The main flow can be heated by means of a 34kW heater placed at the test rig inlet section. After passing through a flow settling device and some flow straightening grids and honeycombs the flow is accelerated in a bell-mouth shaped nozzle to Mach numbers in the order of 0.3. A turbulence grid located about 45 D upstream of the film-cooling holes created a turbulence intensity level of 4% at ejection location. The test plate consists of a polyurethane foam featuring a low thermal conductivity of about 0.1 W/mK. CO_2 was used as coolant to enable density ratio matching. A detailed description of the rig can be found in Gritsch et al. [17]. The test plate features a row of 5 fan-shaped film-cooling holes. Figure 5 shows a sketch of the film cooling hole geometry, while Table 1 reports the main hole geometrical parameters.

D [mm]	*α [°]*	*L/D [-]*	*C/D [-]*	*P/D [-]*	*AR [-]*	*φ_1 [°]*	*φ_2 [°]*	*β [°]*
4.0	30	11.5	2.0	6.0	4.2	7.22	2.33	0.0

Table 1 Hole geometrical parameters

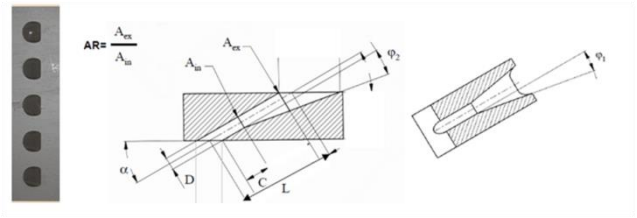

Fig 5 Shaped hole configuration

Tests were performed using both the IR and PSP technique, with coolant to mainstream mass flow ratio (*MFR*) ranging from 0.5% to 2.5% with steps of 0.5%. The IR measurements have been acquired with a FLIR sc6540 IR Camera, (640 x 512 Pixel resolution, 1.5 – 5.1μm spectral range). To minimize the experimental uncertainty, the camera was calibrated in situ, while no conduction correction was applied (i.e. adiabatic conditions were assumed on the plate during the experiments).

In the case of PSP, Uni FIB measurements were performed using the same apparatus already adopted for calibration. The Lavision Imager Pro camera was equipped with Nikkor 60 Micro lenses and a 650/50nm bandpass filter. A second camera, with a 550/50 nm bandpass filter was used to simultaneously acquire the green signal when using the Binary FIB coating. Illumination was provided by the LED UV lamp, operating in flash mode to minimize the aging effect on

the PSP coating during the test campaign. The camera exposure time was set to maximize the signal to noise ratio of the PSP emitted light.

For each testing condition four images were recorded:

- Dark image, i.e. the image without the wind tunnel running and also without illuminating the test surface;
- Wind off image, i.e. an image without the wind tunnel running but illuminating the test surface (this image gives the reference pressure condition, the equivalent of I_{ref} during calibration);
- Air image: a set of 100 images, with the wind tunnel in operation and injecting air;
- CO_2 image: a set of 100 images, with the wind tunnel in operation and injecting CO_2 at the same injecting condition as with air.

For each testing condition, the 100 black and white images were averaged to reduce noise: the resulting mean intensity distributions were converted into pressure values by using equations (8) and (9). This was done pixel per pixel. Similar to Han and Rallabandi [5], wind off and Dark images were collected at the end of testing. Moreover, free stream and coolant temperatures were kept at (25 ± 1)°C thanks to the presence of heaters, in order to limit as much as possible temperature effects. The resulting air and CO_2 pressures were finally used to compute the film cooling effectiveness values through equation (6).

3.2 Results

Figure 6 reports the steady state effectiveness maps and laterally averaged profiles obtained using IR thermometry and single and binary PSP methods. By comparing the contour plots in Fig. 6a it is possible to observe that in the region close to the film cooling hole the PSP technique is showing higher effectiveness values and steeper gradients compared to the IR method. This is a clear effect of thermal conduction, despite the low conductivity of the material used for the test article manufacturing. It has to be observed that conduction has two main effects: first it alters the wall temperature values around the hole and second it modifies the temperature distribution across the jet at hole exit section. In fact, due to heat transfer along the hole, coolant temperature distribution is no more uniform across the jet, with higher values in the middle section and reduced levels at the boundaries. When using PSP technique, a foreign gas is injected, resulting in a 0 oxygen concentration across the hole exit section that would correspond to a uniform temperature distribution. This different behaviour influences the perception of jet traces on the wall given by the two techniques.

Conversely, IR and PSP are in a very good agreement far downstream the hole. This behaviour is better quantified in the lateral averaged distributions shown in Fig. 6b. It has to be noted that, to better appreciate the differences between the two techniques, data were laterally averaged over the hole middle section ($-1 < y/D < 1$) and not over the pitch, as it is common practice. This motivates the averaged effectiveness values of about 1.0 over the hole exit section (also note

that the origin of the coordinate system is located at the hole leading side). Moreover, the reader can observe that the area affected by conduction error in the IR maps is larger with increasing *MFR*, showing discrepancies up to 15 *D* downstream the hole. A more detailed comparison can be done calculating the point-to-point ratio of the effectiveness values obtained with PSP and IR (Figure 7). These data show that the IR method underestimates η at higher η values while overestimates it where the film cooling protection is poor. As stated before, this phenomenon is caused by a non-negligible 2D conduction occurring at the wall.

When comparing the UniFib results with the Binary ones (Fig.6c,d), the reader can observe that the agreement is good, as expected, with some minor differences in the hole exit section, probably due to some residual differences between coolant and mainstream temperature.

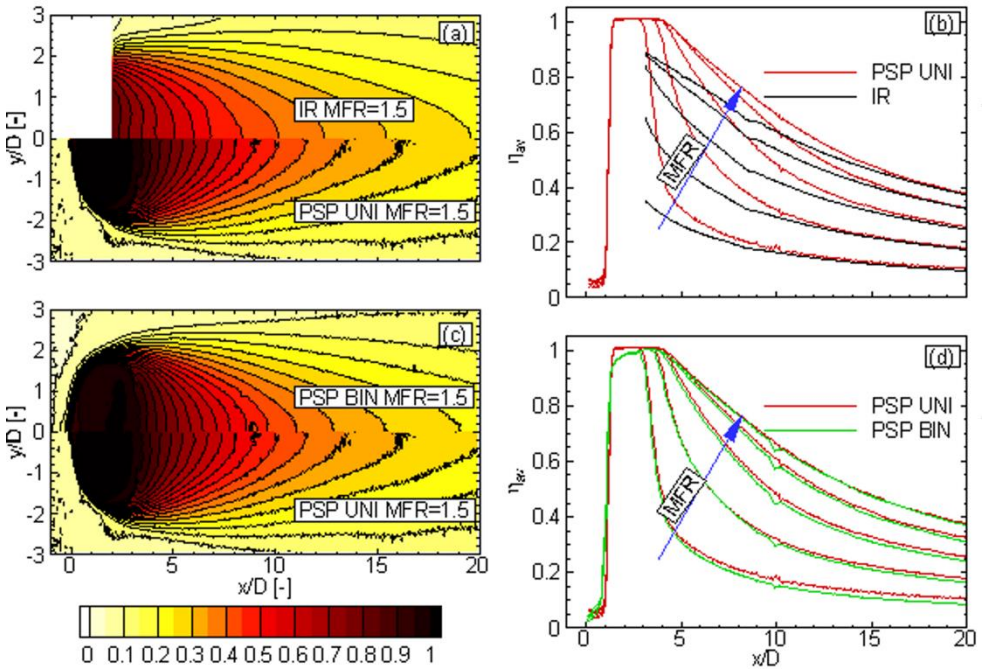

Fig 6 Comparison between IR and PSP results: a) local η distributions from IR and PSP at *MFR* = 1.5%, b) laterally averaged distributions from IR and PSP for variable *MFR*, c) local η distributions from PSP and binary PSP at *MFR* = 1.5% and d) laterally averaged distributions from PSP and binary PSP for variable *MFR*

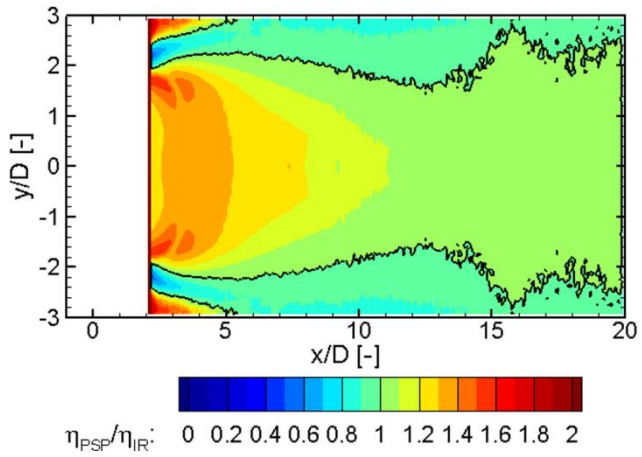

Fig 7 Local distribution of η_{PSP}/η_{IR} - *MFR* = 1.5%

4. THE VANE CASCADE TEST CASE

To fully assess the binary PSP technique, the same methodology successfully tested on the flat plate case was applied to a more complex geometry like the cooling of the pressure side of a high pressure nozzle vane cascade equipped with a cutback trailing edge. This test case was chosen because the same geometry has been extensively tested, both experimentally [22-24] and numerically [25,26], at Bergamo University Laboratory so film cooling effectiveness distributions measured at variable *MFR* and downstream Mach number with the wide banded TLC technique are available for comparison [22]. These tests were considered by the authors very challenging. The complex geometry posed serious limits to the applicability of adiabatic condition in several portion of the investigated domain. In this context, PSP technique can take advantage of this complex flow condition to fully demonstrate its superiority in measuring the film cooling effectiveness distribution when compared to heat transfer based techniques. Moreover, the binary formulation can demonstrate its high flexibility in giving high quality results without the need of controlling temperature.

4.1 Experimental details

Tests were performed in the subsonic wind tunnel for linear cascades at the Turbomachinery Laboratory of Bergamo University, Italy. This is a continuously operating, suction-type wind tunnel equipped with a six-bladed high loaded nozzle vane cascade. Details of cooled cascade geometry have been already presented [23] but are here summarized for clarity (Fig. 8). The pressure side of the vanes is equipped with two staggered rows of cylindrical holes and a cutback trailing edge. Rows are located at x/c_{ax} = 0.52 and x/c_{ax} = 0.64, respectively. Hole diameter *D* is 1.05 mm, hole-to-hole pitch is 2.76*D* and hole length is 4.9*D*. Holes are angled at 30° to the surface. The cutback starts at x/c_{ax} = 0. 72. It consists of eight equally spaced rectangular slots characterized by a slot width to height ratio, *w/H* = 4.7. A rounded lip

was adopted, having a lip thickness to slot height ratio t/H = 1.0. The cooling flow enters the plenum realized inside of the vane from the hub side; after a 90° turning, it is then driven into a channel feeding the holes and the cutback. A rib array was realized inside this feeding channel, as shown in Fig. 8. The span wise rib width is 2 mm and their thickness gradually decreases to zero, at a distance of 8 mm from the vane trailing edge. Holes and cutback are spread over 70% of the vane height.

The cascade was tested at different exit Mach numbers ranging from $Ma_{2,is}$ = 0.2 up to 0.6, corresponding to a $Re_{2,is}$ variation from 6.5×10^5 to 1.6×10^6, and at a low Tu_1 of 1.6% (Table 2). Tests were performed using the binary PSP technique, injecting air and N_2, with the coolant to mainstream mass flow ratio (MFR) ranging from 0.8% to 2.8%.

Binary FIB measurements were performed using the same imaging system already used during calibration. The FlowSense EO 4M camera was equipped with a Nikkor 50mm lens and the sliding filter holder (Fig. 2) hosting a 650/50nm and a 550/50 nm band-pass filters. Illumination was provided by the same 400nm LED UV lamp used in the flat plate experiment, always operating in flash mode to minimize the aging effect on the PSP coating during the test campaign. The camera exposure time was set to maximize the signal to noise ratio of the PSP emitted red light.

The CCD camera was mounted on the wind tunnel inlet section while the UV lamp illuminated the vane pressure side from one side. Some unavoidable shadowing on one side of the ribs took place.

Nevertheless the tested geometry is the same, it has to be observed that previous TLC measurements were performed on vane models manufactured by a rapid prototyping machine while PSP measurements were performed on Plexiglas vanes. This makes some differences in the quality of surfaces, especially the internal ones: smooth in the Plexiglas model, highly rough in the rapid prototyping one.

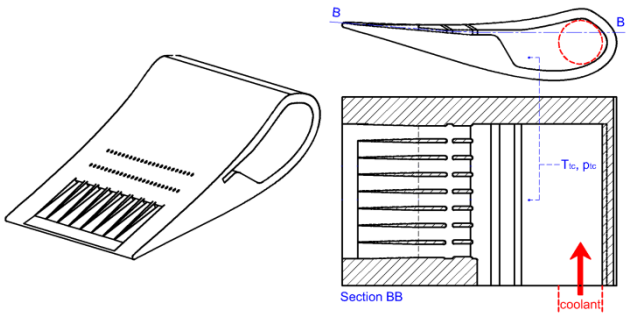

Fig 8 The cooled cascade model

c = 142.1 mm	β_2 = 20°
s/c = 1.04	$Ma_{2,is}$ = 0.2 - 0.6
H/c = 0.69	$Re_{2,is}$ = 6.5 10^5 - 1.6 10^6
th_{TE} = 2.6 mm	Tu_1 = 1.6 %
β_1 = 90°	MFR = 0.8 – 2.8 %

Table 2 Cascade geometry and operating conditions

4.2 Results

Figure 9 shows the results from vane cascade PSP testing on vane pressure side at a low Mach number of 0.2 for variable injection condition from *MFR* = 0.8% to 2.8%. As a general comment, PSP technique is able to capture all relevant phenomena already observed by TLC measurements [22]. In particular, a certain degree of non-uniformity in the span wise direction can be observed, due to the fact that coolant is supplied from one side of the vane (from the right in Fig. 9) and the plenum has a constant cross section along the span. Moreover, the same behavior of coolant ejected from holes for variable *MFR* is also measured: at the lowest injection rate (Fig. 9a - *MFR* = 0.8%) no coolant exits the holes but it can only be discharged through the slot. A small increase in *MFR* (Fig. 9b - *MFR* = 1.1%) allows all systems to come into operation, thus contributing to the thermal protection of the pressure side. Further increasing the *MFR* up to 2.0% (Fig. 9c) coolant discharged from the first row of holes lifts off the wall resulting in a decrease of performance that also involves the second row of holes when *MFR* = 2.8%. This behavior was shown to be consistent with the values of coolant to main stream Blowing Ratio (*BR*) parameter, being 1.0 when jet lift off takes place [23], as reported in Table 3.

MFR (%)	***BR row#1***	***BR row#2***	***BR slot***
1.1	0.45	0.37	0.67
1.3	0.77	0.62	0.71
2.1	1.4	1.12	1.02
2.8	1.9	1.55	1.4

Table 3. Hole and slot injection conditions (*DR* = 1.0)

Shifting attention to the region downstream of the slot and extending up to the trailing edge, again PSP technique captures the typical trend of slot cooling, with thermal efficiency promoted by the increase in *MFR*. As well known, the thermal protection in the cutback region is dominated by the presence of large coherent structures that are shed alternatively from the two sides of the lip, as shown experimentally by Barigozzi et al. [23] and numerically by Ravelli and Barigozzi [25]. When coolant is injected with a low momentum, and thus with a velocity smaller than the main stream one, the main stream side vortical structure dominates driving air towards the wall. The result is a quick decay of film cooling effectiveness right after the slot exit section (Fig. 9a). Progressively increasing the coolant mass flow, and thus velocity, the coolant side vortex gets larger and finally, when coolant velocity becomes large enough, almost suppresses the main stream side vortex, resulting in a thermal protection that persists up to the trailing edge (Fig.9d). It is worthy to observe that η values lower than 1 are detected by PSP technique at slot exit for the lowest tested *MFR* of

0.8%. This is due to main flow ingestion taking place across the holes in this very low injection condition, according to a coolant pressure value measured inside the vane lower than the profile pressure at hole exit.

To better appreciate the advantages of PSP over TLC technique in such a complex geometry, Fig. 10 reports the η distributions measured with the TLC technique at a *MFR* of 1.1% and 2.0%. Upstream of the slot vane thickness is quite small (the lip thickness *t* is 1.4 mm), resulting in a quite relevant conduction affecting TLC results. Moreover, coolant temperature was measured at the inlet of the feeding chamber and not at hole exit section. Finally, due to conduction along the hole, coolant temperature is not uniform across the hole exit section. All these aspects contribute to the computation of smaller η values from TLC, when compared with PSP data.

Moving to the cutback region, the main differences relay in a general underestimation of η by TLC. More in detail, TLC and PSP distributions show a different η behavior in two specific regions: close to slot exit at the low *MFR* of 1.1% and close to the trailing edge at the high *MFR* of 2.0%. The first difference (close to the slot - Fig.9b and 10a) can be explained by considering that, as stated before, TLC measurements were performed on a model manufactured with a rapid prototyping machine while PSP measurements were run on a Plexiglas model. The unavoidable imperfections in the internal geometry and the high roughness of the internal surface of the first model caused a flow separation in the slot exit section at low injection rates, as documented in Ravelli and Barigozzi [26]. This separation was not present in the Plexiglas models, realized by a 4 axis NC machine assuring a precise geometry definition with very smooth internal surfaces. The second difference takes place close to the trailing edge (Fig.9c and 10b), where TLCs show a quicker decay in the film cooling effectiveness while approaching the trailing edge. This again could be due to conduction phenomena as the trailing edge is quite thin (2.6 mm) and to the transient nature of TLC tests. In fact, to limit conduction phenomena, test duration was limited to few seconds: this could have negatively affected the trailing edge region, where thermal steady state condition was hardly reached within the test duration. Please note that test duration was always long enough to assure a steady aerodynamic condition (the response time to reach steady state aerodynamic condition was always well below 0.1s).

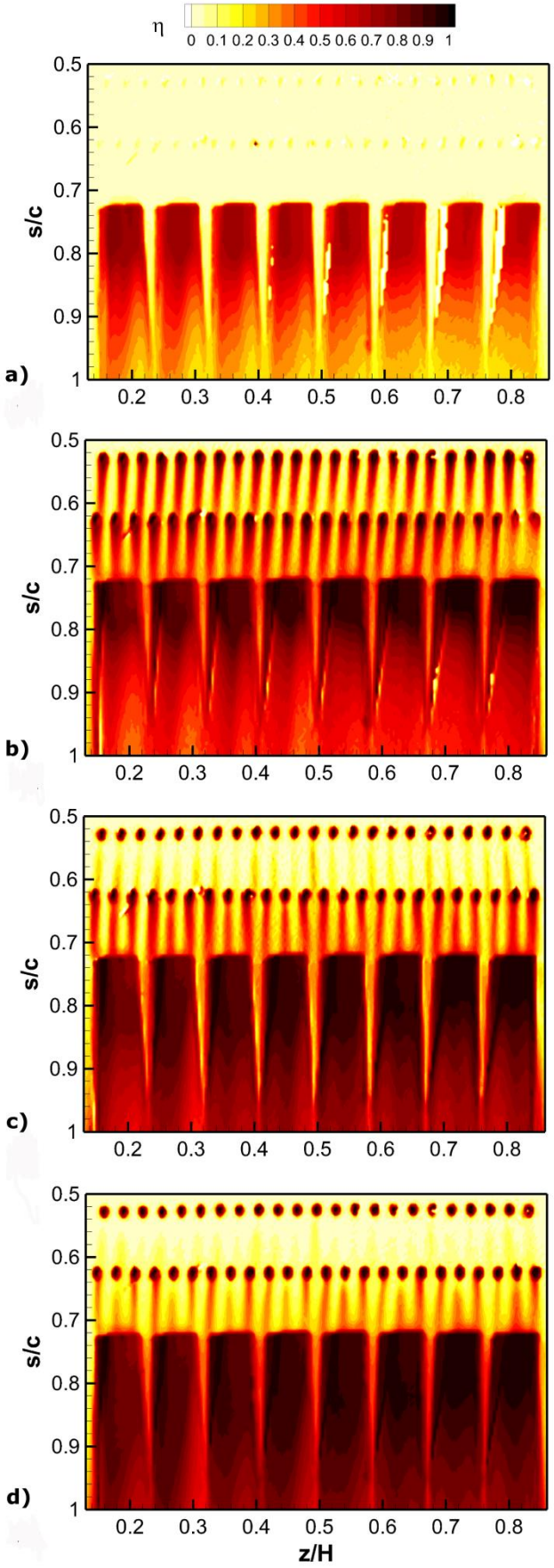

Fig 9 PSP film cooling effectiveness distributions ($Ma_{2,is}$ = 0.2) for variable *MFR*: a) 0.8%, b) 1.1%, c) 2.1% and d) 2.8%

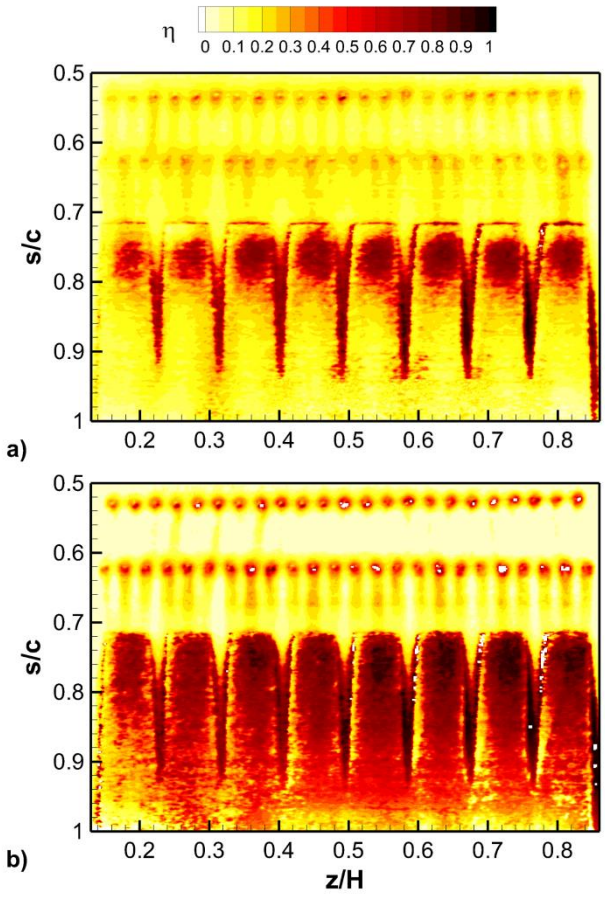

Fig 10 TLC film cooling effectiveness distributions ($Ma_{2,is}$ = *0.2*) for variable *MFR*: a) 1.1% and b) 2.8% [22]

Despite the differences between PSP and TLC results, similar η variations have been detected, as Fig. 11 shows. Both techniques show the existence of an optimal injection condition for the holes around *MFR* = 1.1% and a progressively increasing thermal protection with rising *MFR* over the cutback region, even if TLC technique always shows much lower η_{aa} values when compared with PSP, especially in the cutback region.

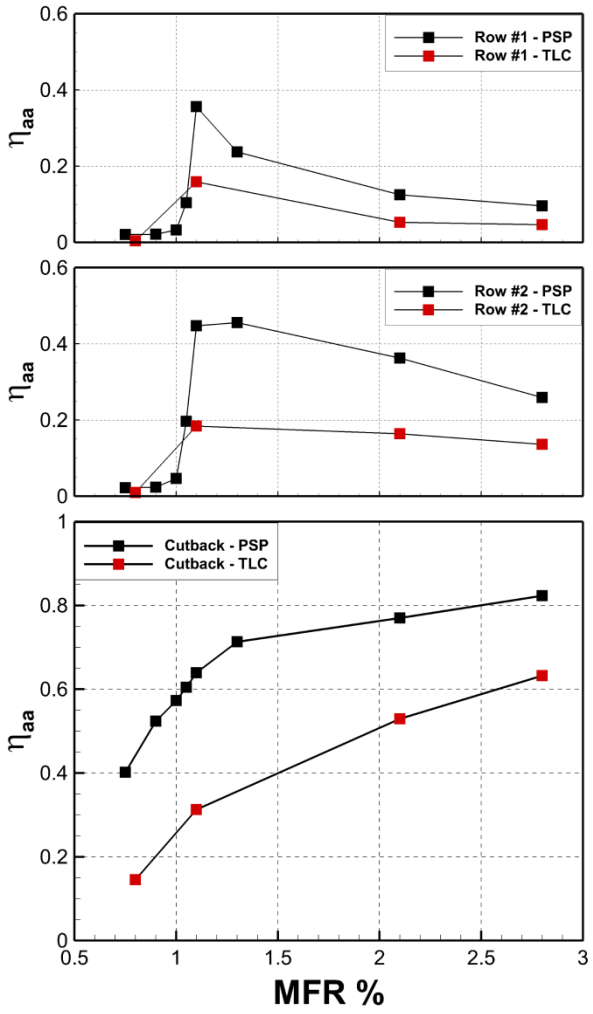

Fig 11 Comparison between binary PSP and TLC area averaged film cooling effectiveness distributions ($Ma_{2,is}$ = 0.2): a) Row#1, b) Row#2 and c) cutback

The huge difference between TLC and PSP data requires a further validation to assess the real accuracy of Binary PSP technique. For this reason, Fig. 12 compares laterally averaged and centerline film cooling effectiveness distributions measured with PSP technique with literature data. Figure 12a refers to the first row of holes, Fig. 12b refers to row#2 while Fig. 12c refers to the cutback region. To make the present data comparable with literature data obtained testing simplified models, the *s/c* coordinate of Fig. 9 has been transformed into a Cartesian coordinate *x* normalized either with the hole diameter *D* or the slot height *H*. Moreover, instead of using the *MFR* parameter, hole data are plotted reporting the corresponding value of blowing ratio *BR* and momentum flux ratio *I*. Data are colored according with the *BR* value: black for low, red for mid and blue for the largest *BR* values. Table 3 shows the correspondence between *MFR* and *BR* for holes and slot.

First considering the η_{av} distributions downstream of row#1 (Fig. 12a), a good agreement between PSP measurements and literature data is observed, whatever the injection condition. Please note that literature data refer to flat plate

investigation and they were selected in such a way to have similar values of hole injection angle, *L/D* and *P/D* parameters. In particular, a good agreement is obtained with both Kholi and Bogard [27] and Foster and Lampart [28] results when considering the same momentum flux ratio *I* rather than the same blowing ratio *BR*, as literature data were collected at a higher density ratio *DR* (1.6 for [27] and 2.0 for [28]). The slightly larger effectiveness level at $x/D > 6$ for the present data can be probably due to the presence of the second row of holes. The present *MFR* = 2.0% injection case corresponds to a *BR* = 1.4 and thus to a *I* of about 2.0, much higher than the value tested by Kholi and Bogard [27]. This is the reason why the present distribution exhibits much lower values.

Moving to row#2, unfortunately a direct comparison with literature data cannot be done in terms of laterally averaged effectiveness, as the computed distribution strongly depends on hole as well as on row spacing. Moreover, in the present case a certain degree of non uniformity in the span wise direction characterizes the jet behavior downstream of this row, (the same stands even for row#1, but with a less intensity), due to the presence of the rib array inside the feeding channel (see Fig. 8). For this reason, centerline effectiveness values were extracted from the three holes located around the vane mid span, averaged and compared with literature data from flat plate testing (Fig. 12b). A good agreement with literature data is observed for low to mid injection conditions. The larger effectiveness level of the high injection case with respect to Gritsch et al. [29] results is consistent with the lower *BR* and *I* values of the present case.

Shifting attention to the cutback region, the comparison is made with literature data coming both from simplified models without mainstream acceleration [11, 30] and cascade data [31]. Martini et al. [30] and Dannhauer [31] configurations have internal ribs that do not extend outside the slot; in both cases IR thermometry was used to measure the film cooling effectiveness distribution. Wong et al. [11] configuration instead does not have any internal obstruction, but it has tapered lands that extend up to $X/H = 12$; in this case PSP technique was used to characterize the slot thermal behavior. Figure 12c shows the laterally averaged distributions of film cooling effectiveness for two injection conditions, corresponding to a slot *MFR* of about 1% and 2%. A very good agreement between the present data and Wong et al. [11] results for both the considered injection cases is observed but for the slot exit region, due to the different internal geometry. A general agreement in terms of η decay downstream of injection and of η increase with *MFR* also takes place when considering Martini et al. [30] data: the lower levels of the present results close to slot exit are due to the presence of external ribs that do not exist in Martini's model. Conversely, the higher persistency of the present distributions going downstream is consistent with the presence of an accelerating main stream, that does not exist in Martini's model. Finally, Dannhauer [31] results show a quicker decay in the downstream direction, even higher when rising the injection rate. This different behavior has to be related to the very low *BR* value of both reported cases, that in turns are due to the presence of a diffusion section inside of the feeding channel.

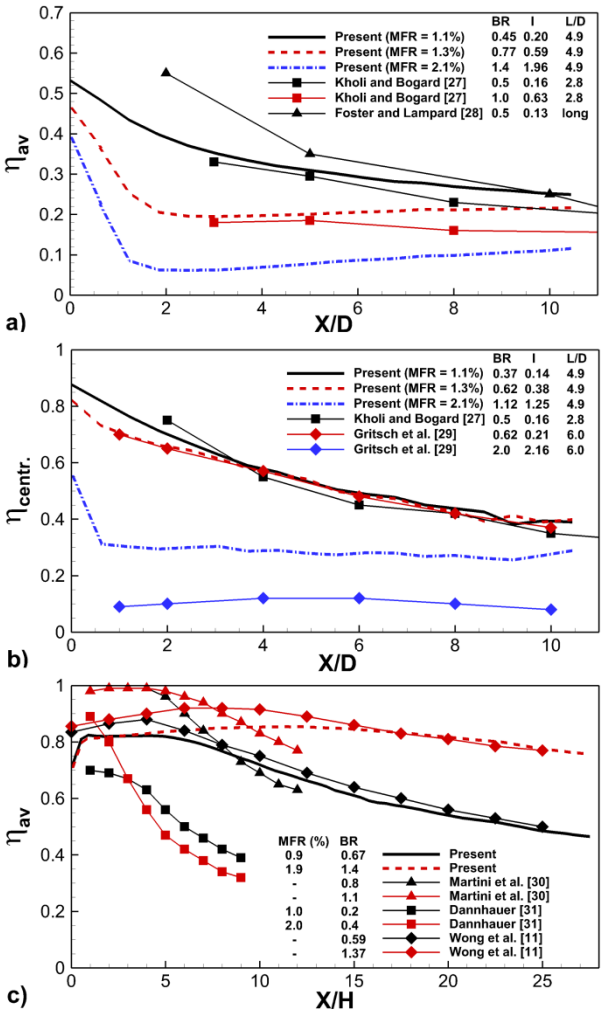

Fig 12 Comparison with literature data: a) Row#1, b) Row#2 and c) cutback

PSP measurements were also repeated for variable exit Mach number. The $Ma_{2,is}$ = 0.6 testing condition was considered a good test case for assessing the influence of temperature variation on binary PSP results, even if the recovery temperature variation along the vane surface in that operating condition was less than 2°C. What was changing is the coolant temperature when injecting nitrogen, due to the strong expansion taking place from the cylinder to holes/slot exit section. As a consequence, a temperature mismatch of about 20°C between cooling (cold nitrogen) and wind off (room temperature) conditions took place, as coolant temperature was only determined by the specific mass flow rate and Joule - Thomson expansion effect (no temperature control was applied to the coolant). Considering the calibration curves reported in Fig. 3, such a (negative) temperature mismatch will result in an underestimation of pressure ratio when injecting nitrogen (if data processing is based on a unique calibration curve, as typically is). This will translate into an overestimation of film cooling effectiveness, according to equation (6). Please note that compressibility effects, if relevant, are expected to act differently, as this time a temperature mismatch will exist between both cooling (air and nitrogen) and reference (wind off) conditions.

To investigate the influence of temperature correction, the processing of binary PSP was repeated without considering the green signal, i.e. like for single component luminophor. In this way, any difference between the two sets of data will be related to temperature. As an example Fig. 13 shows the laterally averaged film cooling effectiveness distributions measured at $Ma_{2,is}$ = 0.6 for two *MFR* values of 1.3% and 2.0% with and without temperature correction. The difference between these two sets of data is also reported in order to quantify the impact of temperature correction (green correction - black line). In the analysis of these data it has to be reminded that temperature influence on PSP signal is higher when η is small and almost disappears when η approaches 1. Temperature correction is in general limited. Generally speaking, the correction is higher in the hole region rather than over the cutback, due to the presence of uncooled or poorly cooled areas. As previously stated, compressibility effects are limited, so the major contribution to temperature variation comes from the mismatch between coolant and main flow. A maximum difference of about 100% occurs upstream of the holes. But in this region film cooling effectiveness is about zero, so the actual value of temperature correction is quite low, about 0.06. The correction nulls or it is quite low where film cooling effectiveness is high, i.e. at hole location and just downstream of the slot. It then increases as soon as oxygen concentration, and thus its partial pressure, increases and film cooling effectiveness decreases. This is particularly evident both in the hole region, where the correction increases increasing the *MFR*, and in the cutback region, where the correction increases going downstream as well as lowering the *MFR*.

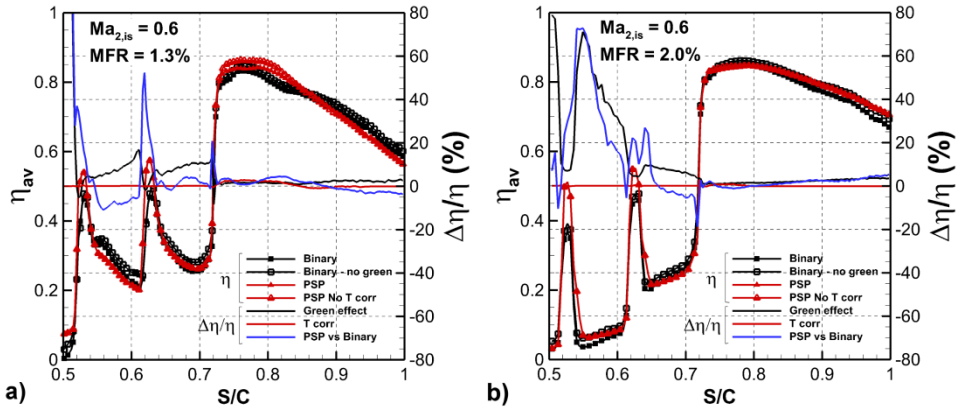

Fig 13 Influence of temperature correction on laterally averaged film cooling effectiveness distributions ($Ma_{2,is}$ = 0.6): a) *MFR* =1.3% and b) MFR = 2.0%

Finally, Fig. 13 also reports data obtained using single luminophor PSP. Wind off images were acquired both before and after the tests, in order to evaluate the impact of temperature correction proposed in [5] on the final result. The impact of this temperature correction (red line) as well as the difference between Binary and single component PSP results (blue

line) are also reported in Fig. 13. Isothermal tests were also run with single component PSP, i.e. heating the coolant to match the mainstream temperature. These data are not reported, as they practically coincide with binary PSP results, when the wind off image is recorded just after the test.

A high degree of consistency characterizes the two sets of data (Binary and single component PSP), with differences between Binary and single component PSP results always in the range of measurement uncertainty. Temperature correction on PSP is always an order of magnitude lower, and it only slightly influences the hole and cutback exit region, where coolant to mainstream temperature mismatch is higher. A stronger impact would be expected where compressibility effect is higher.

4. CONCLUSIONS

A critical assessment of binary PSP technique for the measurement of film cooling effectiveness has been documented in this paper. The experiments have been carried out in two distinct laboratories, allowing to design the necessary calibration setup and to perform calibrations under variable testing conditions. The wide calibration campaign carried out both on single component and binary PSP allowed to verify the effect of parameters like temperature and CCD camera selection on the PSP response. In particular, binary PSP were proven to give a signal almost independent from temperature over a significant temperature range. However, the camera has an impact on the calibration curve, therefore the same camera must be used both during calibration and measurement.

The PSP technique has been then used on a flat plate model with shaped holes and on a nozzle vane cascade with pressure side cooling holes and a cutback trailing edge. In the first test case the comparison with data from IR thermometry gave a good agreement between these two techniques far from injection location. A higher mismatch between PSP and IR technique was observed approaching the holes. This difference increased both in value and extension with rising the injected mass flow. This was ascribed to a non-negligible conduction effect, that was still present notwithstanding the low conductive material used for model manufacturing. The second test case was more challenging for the binary PSP technique, due to the more complex geometry. The binary PSP technique gave high quality results when compared with data measured with wide banded TLCs, completely unaffected by conduction or the uncertainty related to temperature mismatch between coolant and mainstream. Notwithstanding the large difference detected between PSP and TLC local values, the general behavior of film cooling effectiveness with variable injection condition was correctly captured by both measurement techniques, providing an optimal *MFR* of 1.1% for the holes and a continuous increase in the thermal protection of the cutback region with rising *MFR*. Moreover, the comparison between the present results and literature data allowed to fully assess binary PSP technique, demonstrating its superior performance when applied to complex geometries and flow conditions. The high Mach number case with the low

coolant temperature also proved the benefit of binary PSP technique when a good match of temperature cannot be assured for all the actors: coolant, mainstream and model.

References

[1] Han J-C, Dutta S, Ekkad SV (2000) Gas Turbine Heat Transfer and Cooling Technology. Taylor & Francis, New York.

[2] Friedrichs S, Hodson HP (1994) The Ammonia and Diazo Surface Coating Technique for Measuring Adiabatic Film Cooling Effectiveness. 12th Symposium on Measuring Techniques for Transonic and Supersonic Flow in Cascades and Turbomachines. 12-13 September 1994, Prague, The Czech Republic.

[3] Zhang L, Baltz M, Pudupatty R, Fox M (1999) Turbine nozzle film cooling study using the Pressure Sensitive Paint (PSP) Technique. ASME paper 99-GT-196. doi:10.1115/99-GT-196.

[4] Bell JH, Schairer ET, Hand LA, Metha RD (2001) Surface Pressure Measurements Using Luminescent Coatings. Ann. Rev. Fluid Mech. 33:155-206. doi:10.1146/annurev.fluid.33.1.155.

[5] Han J-C, Rallabandi AP (2010) Turbine Blade Film Cooling Using PSP Technique. Frontiers in Heat and Mass Transfer. 1:013001. doi:10.5098/hmt.v1.1.3001.

[6] Li S-J, Lee J, Han J-C, Zhang L, Moon H-K (2016) Turbine Platform Cooling and Blade Suction Surface Phantom Cooling From Simulated Swirl Purge Flow. J. Turbomach. 138(8):081004-081004-11. doi:10.1115/1.4032676.

[7] Wright LM, Gao Z, Varvel TA, Han J-C (2005) Assessment of Steady State PSP, TSP, and IR Measurement Techniques for Flat Plate Film Cooling. Proceedings of HT2005, 2005 ASME Summer Heat Transfer Conference. July 17-22, 2005, San Francisco, CA, USA (Paper n. HT2005-72363). doi:10.1115/HT2005-72363.

[8] Caciolli G, Facchini B, Picchi A, Tarchi L (2013) Comparison between PSP and TLC steady state techniques for adiabatic effectiveness measurement on a multiperforated plate. Exp. Thermal and Fluid Science 48:122-133. doi:10.1016/j.expthermflusci.2013.02.015.

[9] Liu T, Guille M, Sullivan JP (2001) Accuracy of Pressure Sensitive Paint. AIAA Journal 39(1):1-42. doi:10.2514/2.1276.

[10] Natsui G, Little Z, Kapat JS, Dees JE, Laskowski G (2016) A Detailed Uncertainty Analysis of Adiabatic Film Cooling Effectiveness Measurements Using Pressure-Sensitive Paint. J. Turbomach. 138(8):081007-081007-12. doi:10.1115/1.4032674.

[11] Wong TH, Ireland PT, Self KP (2016) Film Cooling Effectiveness Downstream of Trailing Edge Slots Including Cutback Surface Protuberances. Int. J. Turbomach. Propuls. Power 1:4. doi:10.3390/ijtpp1010004.

[12] Yang Z, Hu H (2011) Study of Trailing-Edge Cooling Using Pressure Sensitive Paint Technique. J. of Propulsion and Power 27(3):700-709. doi:10.2514/1.B34070.

[13] Zare-Behtash H, Gongora-Orozco N, Kontis K, Holder SJ (2009) Application of Novel Pressure-Sensitive Paint Formulations for the Surface Flow Mapping of High-Speed Jets. Exp. Thermal and Fluid Science 33:852-864. doi:10.1016/ j.expthermflusci.2009.03.002.

[14] Liu K, Narzary PD, Han JC, Mirzamoghadam AV, Riahi A (2011) Influence of Shock Wave on Turbine Vane Suction Side Film Cooling with Compound-angle Shaped Holes. ASME paper GT2011-45927. doi:10.1115/GT2011-45927.

[15] Zhou W, Johnson B, Hu H (2015) An Experimental Study of Compressibility Effects on the Film Cooling Effectiveness Using PSP and PIV Techniques. 53rd AIAA Aerospace Sciences Meeting. 5-9 January 2015, Kissimmee, Florida, USA. doi:10.2514/6.2015-0352.

[16] Khalil GE, Costin C, Crafton J, Jones G, Grenoble S, Gouterman M, Callis JB, Dalton LR (2004) Dual-luminophor Pressure-sensitive Paint I. Ratio of Reference to Sensor Giving a Small Temperature Dependency. Sensors and Actuators B 97:13-21. doi:10.1016/S0925-4005(03)00484-2.

[17] Gritsch M, Colban W, Schär H, Döbbeling K (2005) Effect of Hole Geometry on the Thermal Performance of Fan-Shaped Film Cooling Holes. J. Turbomach.127(4):718-725. doi:10.1115/1.2019315.

[18] Jahanmiri M (2011) Pressure Sensitive Paints: The Basic and Applications. Research Report 2011:07; Chalmers University of Technology, Goteborg, Sweden.

[19] McLean D (1998) Referenced pressure paint and the ratio of ratios. In: Proceedings of the Sixth Annual Pressure Sensitive Paint Workshop. The Boeing Company. Seattle, Washington, pp. 11–1:35.

[20] Liu T, Sullivan J P (2005) Pressure and Temperature Sensitive paints. Springer, Berlin.

[21] Innovative Scientific Solutions Inc. Binary Pressure-Sensitive Paint (www.psp-tsp.com). Accessed 5 May 2017.

[22] Barigozzi G, Perdichizzi A, Ravelli S (2012) Pressure Side and Cutback Trailing Edge Film Cooling in a Linear Nozzle Vane Cascade at Different Mach Numbers. J. Turbomach. 134(5):051037-051037-10. doi:10.1115/1.4004825.

[23] Barigozzi G, Armellini A, Mucignat C, Casarsa L (2012) Experimental Investigation of the Effects of Blowing Conditions and Mach number on the Unsteady Behavior of Coolant Ejection through a Trailing Edge Cutback. Int. J. Heat and Fluid Flow 37:37-50. doi:10.1016/j.ijheatfluidflow.2012.07.001.

[24] Barigozzi G, Ravelli S, Armellini A, Mucignat C, Casarsa L (2013) Effects of injection conditions and Mach number on unsteadiness arising within coolant jets over a pressure side vane surface. Int. J. Heat and Mass Transfer 67:1220-1230. doi:10.1016/j.ijheatmasstransfer.2013.09.007.

[25] Ravelli S, Barigozzi G (2014) Application of Unsteady CFD Methods to Trailing Edge Cutback Film Cooling. J. Turbomach. 136: 121006-121006-11. doi:10.1115/1.4028238.

[26] Ravelli S, Barigozzi G (2014) Adiabatic and Conjugate Simulations on Flow Field in a Gas Turbine Vane with Pressure Side Film Cooling and Trailing Edge Cutback. Proc IMechE Part A: J Power and Energy 228(6):657-673. doi:10.1177/0957650914532267.

[27] Kholi A, Bogard DG (1997) Adiabatic Effectiveness, Thermal Fields, and Velocity Fields for Film Cooling With Large Angle Injection. J. Turbomach. 119: 352-358. doi:10.1115/1.2841118.

[28] Foster NW, Lampard D (1980) The Flow and Film Cooling Effectiveness Following Injection through a Row of Holes. J. Eng. Power 102(3):584-588. doi:10.1115/1.3230306.

[29] Gritsch M, Schulz A, Wittig S, (1998) Adiabatic Wall Effectiveness Measurements of Film-Cooling Holes with Expanded Exits, J. Turbomach. 120(3): 549-556. doi:10.1115/1.2841752.

[30] Martini P, Schulz A, Bauer HJ (2006) Film Cooling Effectiveness and Heat Transfer on the Trailing Edge Cut-Back of Gas Turbine Airfoils with Various Internal Cooling Designs. J. Turbomach. 128(1): 196-205. doi:10.1115/1.2103094.

[31] Dannhauer A., 2009, Investigation of Trailing Edge Cooling Concepts in a High Pressure Turbine Cascade – Analysis of the Adiabatic Film Cooling Effectiveness, ASME Paper GT2009-59343. doi:10.1115/GT2009-59343.

Nomenclature

AR	area ratio
$BR = \rho_c U_c / \rho_e U_e$	coolant to main stream blowing ratio
c	blade chord, concentration
D	hole diameter
D_{AB}	molecular diffusion
$DR = \rho_c / \rho_e$	coolant to main stream density ratio
h	convective heat transfer coefficient
H	vane or slot height
I	light intensity or
$I = \rho_c U_c^2 / \rho_e U_e^2$	coolant to main stream momentum flux ratio
K	Stern-Volmer constant
L	rib or hole length
Le	Lewis number
m	mass flow rate
Ma	Mach number
$MFR = m_c / m_e$	coolant to main stream mass flow ratio
MM	molecular weight
p	pressure
P	hole pitch
Pr	Prandtl number
q	heat flux
r	light intensity ratio
$Re_{2is} = U_{2is} \cdot c/\upsilon$	isentropic outlet Reynolds number
s	vane pitch, curvilinear coordinate
S	Henry's law constant
Sc	Schmidt number
t	lip thickness
th_{TE}	trailing edge thickness
T	temperature
Tu = u'/U	turbulence intensity

U	flow velocity
u'	root mean square velocity along streamwise direction
X	mole fraction
x,y,z	cascade coordinate system
w	slot width
α	thermal diffusivity or injection angle
β	flow angle (axial direction)
η	film cooling adiabatic effectiveness
ρ	density
ν	cinematic viscosity

Subscripts

1	inlet
2	exit
aa	area averaged
av	laterally averaged
aw	adiabatic wall
ax	axial direction
c	cooling flow
e	main stream
is	isentropic condition
w	wall

List of Figure captions

Fig 1 Calibration setup: a) at Bergamo Lab and b) at Birr Lab

Fig 2 The filter holder

Fig 3 Calibration curves: a) single component and b) binary PSP

Fig 4 Comparison between binary PSP calibration curves from Birr and Bergamo Laboratories

Fig 5 Shaped hole configuration

Fig 6 Comparison between IR and PSP results: a) local η distributions from IR and PSP at *MFR* = 1.5%, b) laterally averaged distributions from IR and PSP for variable *MFR*, c) local η distributions from PSP and binary PSP at *MFR* = 1.5% and d) laterally averaged distributions from PSP and binary PSP for variable *MFR*

Fig 7 Local distribution of η_{PSP}/η_{IR} - *MFR* = 1.5%

Fig 8 The cooled cascade model

Fig 9 PSP film cooling effectiveness distributions ($Ma_{2,is}$ = 0.2) for variable *MFR*: a) 0.8%, b) 1.1%, c) 2.1% and d) 2.8%

Fig 10 TLC film cooling effectiveness distributions ($Ma_{2,is}$ = 0.2) for variable *MFR*: a) 1.1% and b) 2.8% [19]

Fig 11 Comparison between binary PSP and TLC area averaged film cooling effectiveness distributions ($Ma_{2,is}$ = 0.2): a) Row#1, b) Row#2 and c) cutback

Fig 12 Comparison with literature data: a) Row#1, b) Row#2 and c) cutback

Fig 13 Influence of temperature correction on laterally averaged film cooling effectiveness distributions ($Ma_{2,is}$ = 0.6): a) *MFR* =1.3% and b) MFR = 2.0%

List of Table captions

Table 1 Hole geometrical parameters

Table 2 Cascade geometry and operating conditions

Table 3 Hole and slot injection conditions (DR = 1.0)